Strengthening of brick infilled RC frames with different aspect ratios by means of CFRP overlays

Sevket Ozden[1,*], Savas Atmaca[2] and Cengiz Karakoc[3]

[1] Department of Civil Engineering, Kocaeli University,
41380 Umuttepe, Kocaeli, Turkey,
e-mail: sevketozden@yahoo.com
[2] Consultant Engineer, 35370 Yesilyurt, Izmir, Turkey
[3] Department of Civil Engineering, Bogazici University,
34342 Bebek, Istanbul, Turkey

*Corresponding author

Abstract

Post earthquake field investigations reveal that frames with inferior detailing are vulnerable to seismic actions. The presence of a large building stock in Turkey, which is vulnerable to an imminent earthquake, entails fast, relatively easy, and feasible alternative strengthening methods. In this paper, the strengthening of brick infilled walls with fiber reinforced polymer (FRP) overlays, and integrating them to the load carrying system of the frame, is considered as an alternative method for building upgrading. The effectiveness of the FRP overlays on frames with different aspect ratios, is an issue to be investigated. For this purpose, three reinforced concrete (RC) frame specimens with one-third scale and infilled with hollow clay tile (HCT) were strengthened with FRP overlays. The frame specimens had a single bay and two stories, and were tested to failure. The strengthening scheme was shifted, depending on the aspect ratio of the specimens. Test results were evaluated in terms of base shear-roof drift hysteretic response, and a macro model using the well-known equivalent diagonal strut concept was proposed to predict the lateral capacity and the response of the strengthened frames. The model predicted secant stiffness and failure load in an acceptable accuracy range. Theoretical and experimental results proved that aspect ratio significantly affects the level of strengthening attained. The study presented here is part of a comprehensive research work on the strengthening of HCT infilled RC frames, with different aspect ratios by means of various carbon fiber reinforced polymer (CFRP) schemes.

Keywords: aspect ratio; brick masonry infilled frames; CFRP; equivalent diagonal strut; hysteretic response; reinforced concrete; strengthening.

1. Introduction

Strengthening of vulnerable structures to a severe earthquake with fiber reinforced polymer (FRP) materials is a relatively new and a challenging issue. The presence of masonry infills in reinforced concrete (RC) structures influences the behavior significantly. Masonry infills are sometimes beneficial, in that they can decrease the lateral deformations and limit the inter-storey drifts. In addition, they can enhance the load carrying capacity of buildings. By contrast, masonry infills may result in some torsional irregularities, short column effects and soft storey mechanisms. Since the problem is complicated, engineers generally disregard the infills in the analysis and design stages. Neglecting masonry infills in the nonlinear analysis may lead to serious errors in regard to the stiffness and lateral strength of the structure. Hence evaluation mistakes of the performance of the structural elements appear.

Available literature on FRP-strengthened masonry panels indicated that FRP improved the performance of the strengthened infill panels in terms of the shear strength and the load carrying capacity under both in plane and out of plane loading [1–5]. Also, FRP decreased the hollow clay tile (HCT) flaking at extreme conditions [5, 6] and resulted in more reliable behavior. Good mechanical properties such as a high modulus of elasticity and ease of installation facilitate the use of FRP for strengthening purposes of buildings. Moreover, application of FRP results in minimum disturbance to dwellers, eliminating or minimizing the evacuation of residents and shorter construction time.

In the last decade, various studies on FRP-strengthened infilled frames were performed [7–10]. Frame and infill types, FRP orientation and number of layers, and strengthening scheme were some of the investigated parameters. In addition, various mathematical models incorporating micro modeling and macro modeling were presented [7–9, 11].

In this study, three, single-span and two-storey, one-third scale HCT infilled RC frames with three different aspect ratios were tested under quasi-static reversed cyclic loading up to the failure. Inadequate lap splice lengths in columns at the floor levels (20 ϕ, 20 times the longitudinal bar diameter) and in beam bottom reinforcement, plain bars, poor confinement and low quality concrete, hooks with 90° ends, no transverse steel at the joints and strong beam-weak columns were some of the observed deficiencies in the pre-1998 Turkish construction practice. Thus, all frames had these common deficiencies. Carbon fiber reinforced polymer (CFRP) overlays are applied on both sides of the masonry walls and anchored to the surrounding RC frame by means of CFRP anchors. The same technique was also used by some other researchers and proved that it is an efficient, convenient and time saving method for the earthquake-prone infilled frames [12, 13]. A new mathematical model for FRP strengthened infill panels is proposed, including the aspect ratio effect of the frames. The model is based on the well-known equivalent compression strut concept and is implemented into the mathematical model by replacing the infill panel with a single compression

strut. The main objective of this paper is to show the effect of aspect ratio on the behavior of the FRP-strengthened infilled frames and to propose a novel, simple, fast, and efficient macro model for masonry infills. The test results are compared with analytical ones and the global behavior of the specimens is replicated satisfactorily.

2. Experimental program

Three one-third scale, two-storey and single-bay CFRP-strengthened specimens (SA1.0-CV, SA1.7-CVs and SA2.3-CCM) were tested under reversed cyclic quasi-static loading. S and A, in specimen naming, represent the specimen and the aspect ratio, respectively. The number after the acronym A stands for aspect ratio of the specimens, where the aspect ratio of the specimen is defined as the ratio between the frame bay width and the storey height. C and V show that the CFRP strengthening scheme includes cross diagonal and vertical overlays on the infill. The letter "s" in specimen SA1.7-CVs, apart from the type of strengthening scheme, shows the order of the specimen (second) in the set of specimens, with an aspect ratio of 1.7, of which the companion specimen is published elsewhere [14]. CM represents coarse meshes created by the diagonally placed fabrics.

Material properties related to concrete, longitudinal and transverse reinforcement, brick infill (excluding plaster) and the CFRP are given in Table 1. As indicated in Table 1, low quality concrete was used for all specimens to replicate the prototype frame buildings. ASTM C39-96 [15] and ASTM E447-97 [16] standards were used to measure the compressive strength of the concrete and masonry prisms. The compressive strength values of HCTs were determined considering the gross area of the bricks. HCTs were laid flush to one face of the RC frame, and the hollow cores were laid perpendicular to the bed joints. The width, height and length of the hollow clay units were 70 mm, 90 mm, and 86 mm, respectively. Bricks had six hollow cores, each of which had a cross-section of 20×24 mm. The placement of the bricks flush to one face of the frame could have resulted in some torsional problems and increased the possibility of out-of-plane failure of the masonry wall due to the difference between the loading plane and the infill plane. However, out-of-plane failure of masonry was not observed during the experiments.

Cross-sectional dimensions of the columns and beams are the same for all specimens. Dimensions and reinforcement detailing for the specimens SA1.0-CV, SA1.7-CVs and SA2.3-CCM are shown in Figure 1. Plain bars were used for longitudinal and transverse reinforcement. The spacing of transverse reinforcement and the number of longitudinal bars for beams and columns are also given in Figure 1. Diameters of the longitudinal and transverse reinforcement were 8 mm and 4 mm, respectively.

The frame was in a horizontal position when the concrete was cast and cured. Later, frame specimens were lifted up and positioned as prototype buildings. HCTs were laid, and the infill was plastered when the frame was vertical. The thickness of the brick wall was 70 mm and the average thickness of the plaster

for specimens SA1.0-CV, SA1.7-CVs and SA2.3-CCM, were 8.5 mm, 9.5 mm and 9 mm, respectively. Completion of brickwork and plastering was followed by the CFRP application. Hand lay-up technique (dry lay-up) was used to apply CFRP on the infilled frames. In this application, two-component epoxy impregnation resin was first applied on the substrate. Later, CFRP fabric was directly applied onto the epoxy resin. The application of CFRP fabric was followed by squeezing the resin out between the rovings of the fabric by using a laminating roller. Two-component epoxy impregnation resin and unidirectional CFRP overlays were used for the strengthening process. The widths of the cross diagonals and vertical strips were 20 cm and 5 cm, respectively. On the corners of the masonry panels, two layers of CFRP flag sheets, of which fiber directions were perpendicular to each other, were glued to the wall prior to the application of the cross diagonals and vertical strips. These CFRP flags were aimed at improving the crushing strength of the masonry panel and to eliminate the early crushing failure at the panel corners. Specimen SA2.3-CCM had two additional perpendicular layers of flag sheets at the middle part of the specimen, due to the specified strengthening scheme, to eliminate the possible shear failure of beams where cross diagonals were anchored. The fiber direction of the first layer of the CFRP flags was horizontal. Except for the flag sheets, all the diagonal and vertical CFRP sheets were single ply for all specimens. The strengthening scheme of SA1.0-CV and SA1.7-CVs were identical, whereas the strengthening scheme of specimen SA2.3-CCM had only cross diagonals. The strengthening scheme and anchorage details of the specimens are depicted in Figures 2–5. It should be noted, that detail A of specimen SA2.3-CCM is inclined, as shown in Figure 4. Moreover, the sheet dimensions of CFRP anchors and the depths of the predetermined holes are listed in Table 2. The diameter of the anchor holes was 12 mm all over the specimens. The strips and cross diagonals were anchored to the surrounding frame by using CFRP anchor dowels. In addition, CFRP strips and cross diagonals on each side of the infill wall were anchored to the HCT wall via the holes passing through the infill, in order to decrease the possibility of premature debonding, and to increase the bonded length (Detail C in Figure 5). Thus, the possibility of attaining the full capacity of CFRP overlays could be realized. Anchor holes were drilled to the predetermined depth. Moreover, the holes were cleaned with an air compressor from dust, grease or inconvenient materials, such as loose concrete pieces, to improve the bond between concrete and epoxy impregnated CFRP anchors. The manufacturer's recommendations were followed for the preparation of the surface, mixing of the epoxy resin and the CFRP application. In order to allow for the curing of the bonding agent, epoxy, specimens were kept in the laboratory for 14 days before testing.

3. Test setup and instrumentation

All specimens were tested vertically, as shown in Figure 6. The test setup includes a 2000 kN capacity reaction wall, a 250 kN/$\pm$100 mm capacity dynamic actuator, an auxiliary steel frame to restrain the out-of-plane movement of the

Table 1 Material properties.

| Material	Property	SA1.0-CV	SA1.7-CVs	SA2.3-CCM
Concrete	f_c' (MPa)	8.9	10.2	16.0
ϕ 8 Steel (D_b=8 mm)	f_{yk} (MPa)	347	347	347
(longitudinal)	E_s (MPa)	195000	195000	195000
ϕ 4 Steel (D_b=4 mm)	f_{ywk} (MPa)	241	241	241
(transverse)	E_s (MPa)	198600	198600	198600
Masonry	f_{bm} (MPa)	4.44	4.60	5.00
	f_p (MPa)	5.2	6.7	10.5
CFRP	t_{Fiber} (mm)	0.13	0.13	0.13
	f_{ult} (MPa)	3500	3500	3500
	ε_{ult} (MPa)	0.015	0.015	0.015
	E_{Fiber} (MPa)	230000	230000	230000

specimen, vertical and horizontal spreader beams to apply both horizontal and vertical loads, respectively, and a hydraulic ram to provide vertical loading onto the columns. Vertical and horizontal loads were applied independently. As indicated in Figure 6, a horizontal load was applied through a spreader beam in such a way that one-third of the actuator load goes to the first floor. The applied vertical loads on the columns were applied prior to the lateral loads and kept constant throughout testing at an approximate level of 10% of the column capacity; 11% (14.5 kN), 10% (15 kN) and 10% (24 kN) for specimens SA1.0-CV, SA1.7-CVs and SA2.3-CCM, respectively. The horizontal component of the vertical load counted for the base shear calculations.

All lateral displacements, either in-plane or out-of-plane, were measured relative to the base of the specimen. Shear deformations within the panels were measured with electronic linear variable differential transducer (LVDT), while the strain in the CFRP strips, either vertical or diagonal, was measured by strain gauges as shown in Figure 6. Electronic displacement and strain measurements, along with the actuator load and the level of gravity load, was traced with a sixty channel data acquisition system.

3.1. Testing procedure

The loading history affects the behavior of reinforced concrete frames, especially in the nonlinear range. In order to flatten the response differences between specimens arising from the loading history, ACI T1.1-01 [17] was used in the test of the specimens. The loading history proposed by the
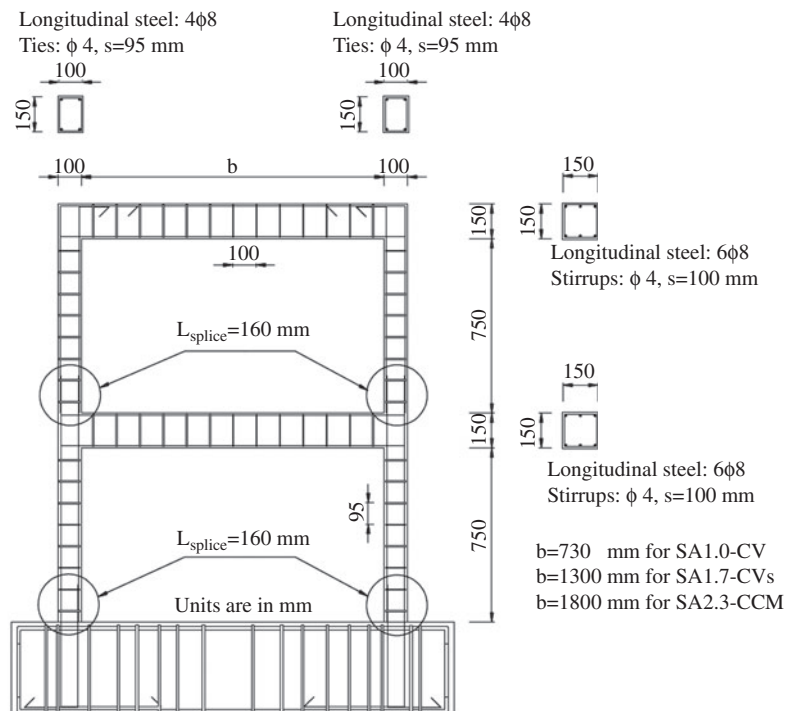
Figure 1 Reinforcement detail of specimens.

ACI T1.1-01 can easily be applied for specimens or sub-assemblies that will fail under flexure. On the other hand, the specimens of the current investigation with HCT infills experienced a mixed type of failure, before the failure load was reached. The stiffness of the specimens was very high, resulting in very small inter-storey drifts that might not be responded by the electronic control system of the hydraulic actuator. Therefore, load controlled type of loading was used at the initial stages of the testing. In the meantime, inter-storey drift values of each load level were compared with the drift levels specified by the ACI T1.1-01 procedure. Whenever the displacement obtained from the load controlled segment of the loading coincided with the displacement dictated by ACI T1.1-01, the loading regime was shifted from the load controlled pattern to the displacement controlled type of loading.

The ratio between two consecutive drift amplitudes of the ACI T1.1-01 procedure was in the range of 1.25 to 1.50 and three full reversed cycles were applied at each displacement amplitude. When the load controlled type of loading was used, it was intended to avoid softening caused by loading repetitions. That is why previously determined displacement amplitudes and drift ratios obtained at each load controlled phase, were checked at each drift ratio and the decision was made to shift from the load controlled type of loading to the displacement controlled type of loading. The loading

increments were approximately 5 kN for the load controlled phase. The horizontal loading regime patterns for specimens SA1.0-CV, SA1.7-CVs and SA2.3-CCM are given in Figures 7–9, respectively. It should be noted that three full cycles, either load controlled or displacement, were applied at each amplitude level.

4. Experimental results

Observations made during the tests, along with the behavior and failure modes of the specimens subjected to quasi-static reversed cyclic loading, are summarized below. The test results are discussed in a concise manner. The terms front, back, inner face, outer face, and base (Figure 6) were used to define the crack locations.

4.1. Specimen SA1.0-CV

The aspect ratio of this CFRP strengthened specimen was 1.0. The axial load on the columns was approximately 11% of the axial load capacity of the columns. The first visible hairline crack was observed in the backward half cycle (pull direction) on the left column outer face and located approximately 400 mm above the base, where the column clear height is 750 mm. The load level was -22.2 kN, and the corresponding drift level
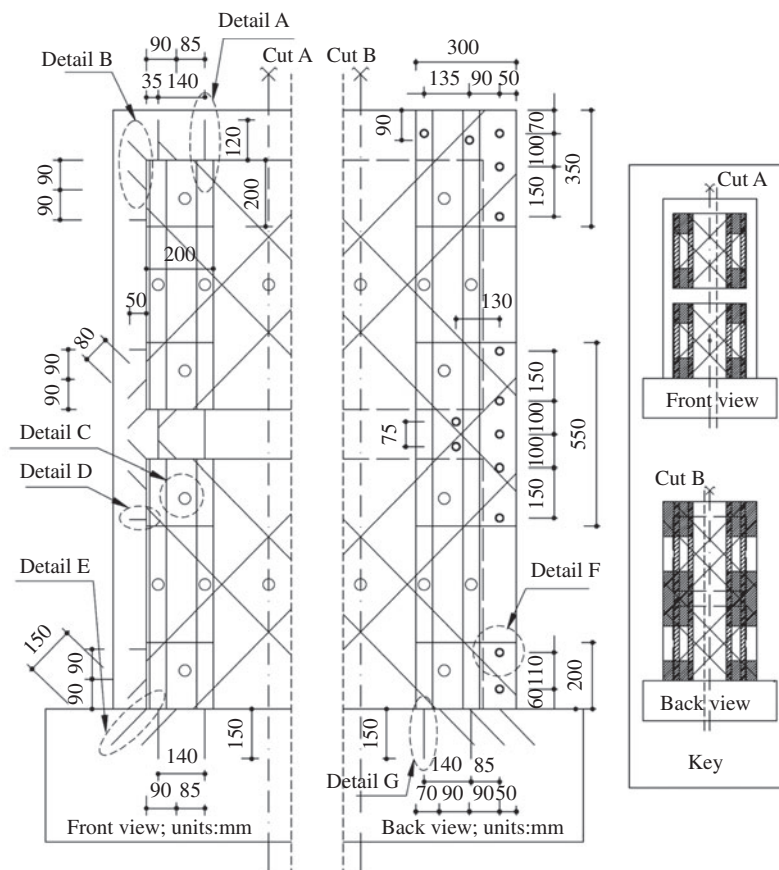
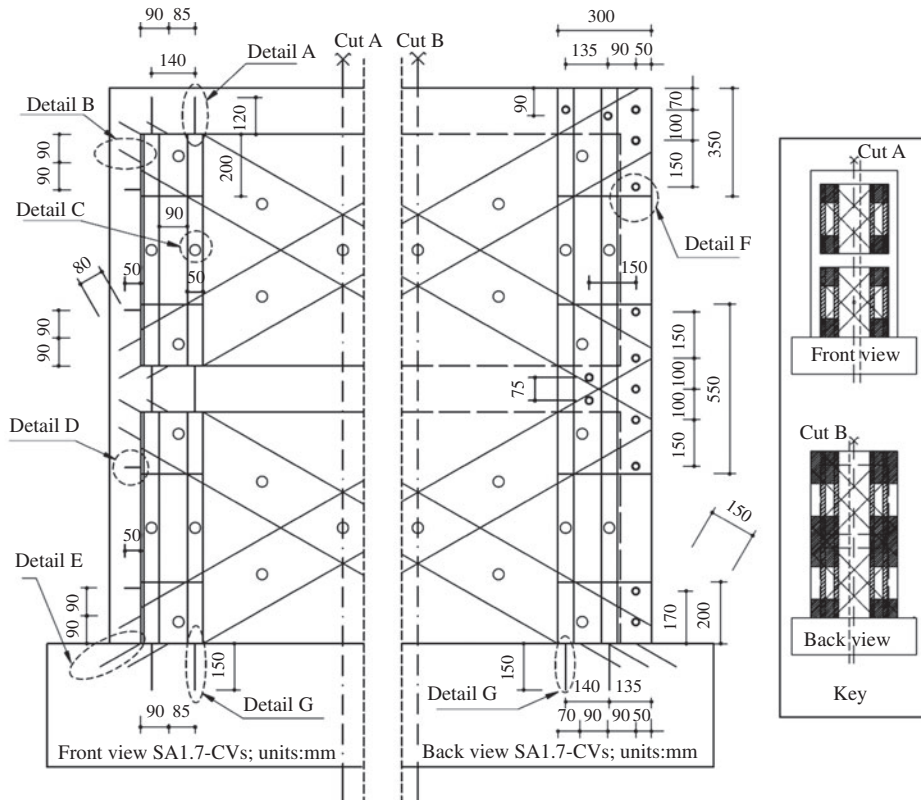**Figure 2**   Strengthening details of specimen SA1.0-CV.

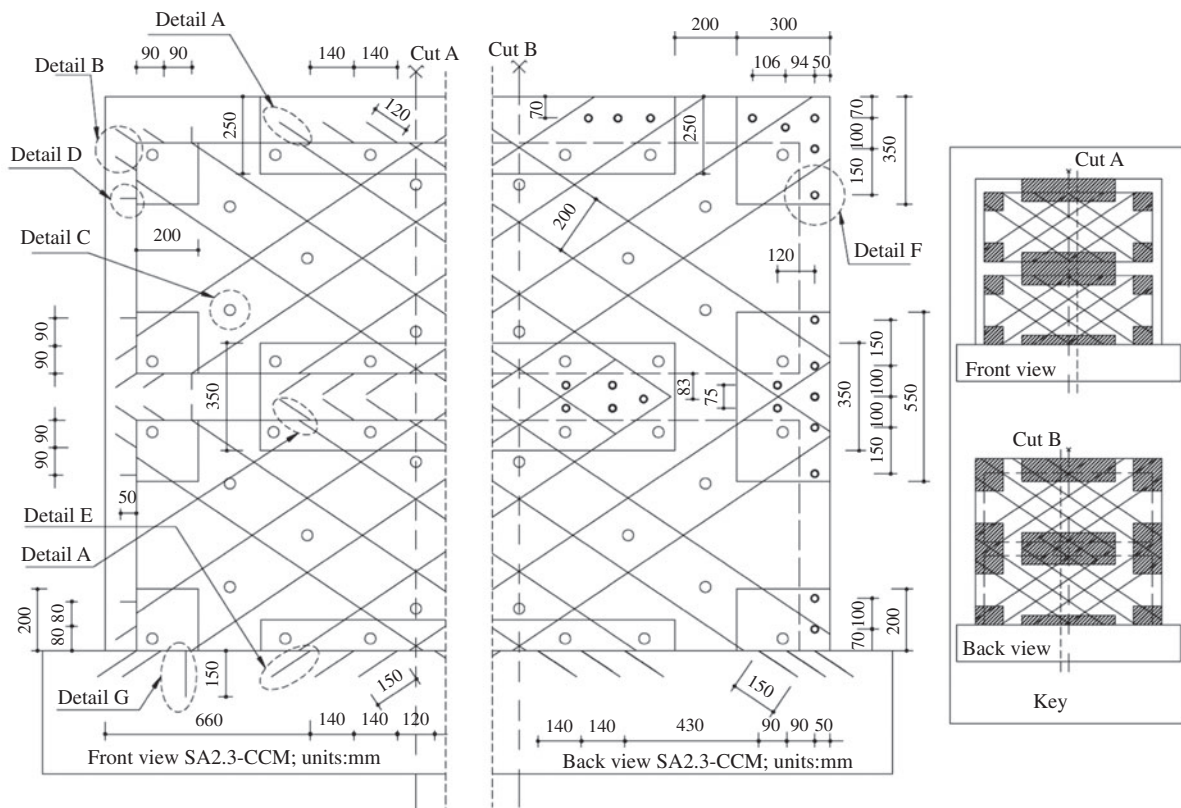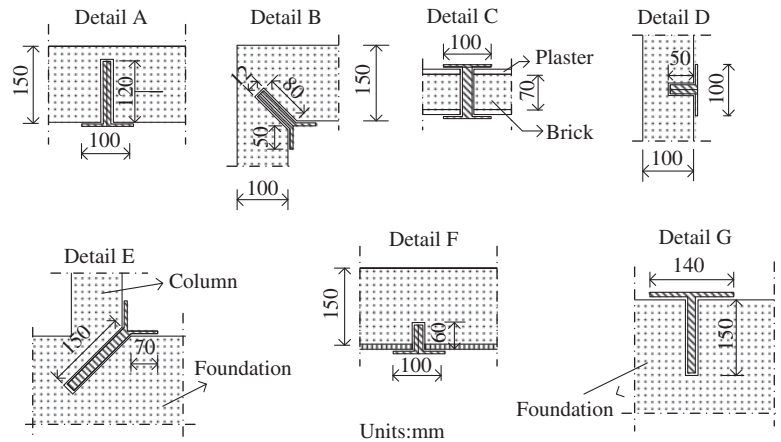**Figure 3** Strengthening details of specimen SA1.7-CVs.

Figure 4 Strengthening details of specimen SA2.3-CCM.

Figure 5 Anchor details.

was approximately -0.049%. The occurrence of the first cracking indicated the lower bound of nonlinear behavior as well as the energy dissipation. Formation of new cracks and the propagation of the existing cracks on the surrounding frame occurred during the subsequent drift ratios. The first cracking on the masonry panel was horizontal and took place at the mid-height region of the first storey panel between the vertical strips. This horizontal crack materialized at the 8th backward half cycle. Besides, the first cracking signs between the first storey panel and the beam were also observed at the same cycle. Such a crack implied the initial separation between the frame and the HCT infill wall. The maximum push and pull loads and corresponding drifts of the 8th cycle were 38.5 kN (0.15% drift) and -40.8 kN (-0.15% drift), respectively. Peak loads that the specimen resisted in the forward and backward cycles, were 58.0 kN (0.771% drift) and -60.0 kN (-0.719% drift), respectively. Thus, the ratio between the maximum load attained at the 8th cycle (when the infill panel separated from the surrounding frame) and the peak load was approximately 68%. Formation of cracks in the infill panel resulted in an energy dissipation and in stiffness deterioration concurrently.

Failure of the specimen is attributed to the tensile failure of columns at the lap splice region, and rupturing of the vertical FRPs under the axial FRP stresses, as shown in Figure 10. When the specimen reached its peak load, severe strength degradation was observed, especially in the backward half cycle. However, a relative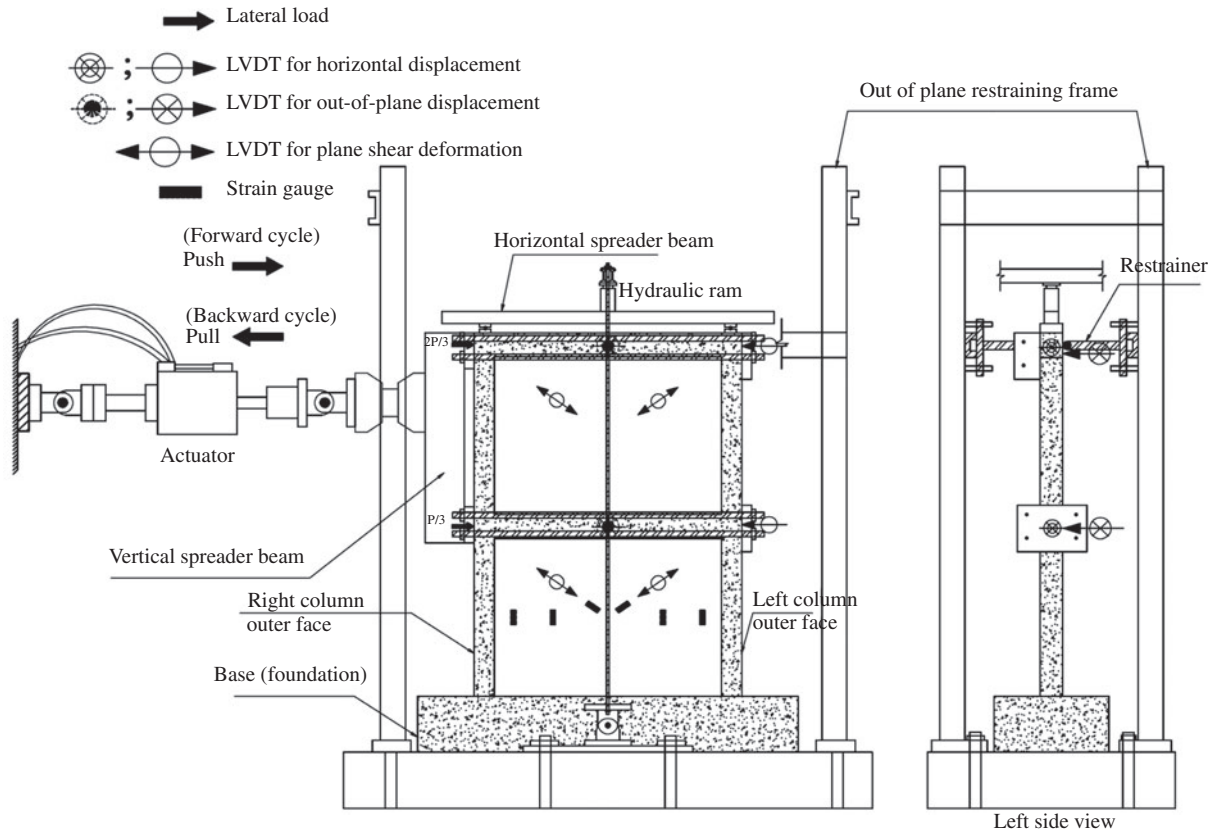ly sequential rupture was observed in the forward half cycle, as can be noticed from the base shear-roof drift diagram in Figure 11. Separation between infill and columns was significant in the post peak region. First storey masonry infill horizontally separated into two main parts, due to the mid-height rocking action of the specimen after rupturing of the vertical FRPs. Besides, the formation of horizontal cracks on the infill implied a horizontal movement of the frame. Spalling of unconfined concrete was observed, especially at the bottom ends of the columns around the lap splice region. Although the specimen failed with the rupture of vertical FRP strips, the top deformation of the frame was influenced by a sliding shear type of deformation that took place at the mid-height of the first storey. This resulted in a so called pseudo-ductility, and the anticipated pinching behavior in the hysteretic loops.

4.2. Specimen SA1.7-CVs

The aspect ratio of this CFRP strengthened specimen was 1.7. The first visible hairline cracks were observed in the 4th cycle at the lower ends of the first storey columns' outer faces, during the forward and backward half cycles. Corresponding applied loads and drift values in the forward (push direction) and backward (pull direction) half cycles were approximately 36.0 kN (0.04% drift) and -35.6 kN (-0.04% drift), respectively. The first crack on the masonry panel was an inclined crack, which was between the first storey beam and the FRP cross diagonal. The maximum pull load and corresponding drift at this

Table 2 CFRP overlay dimensions used for anchors.

Specimens	Anchor detail	Depth of anchor hole (mm)	Width of CFRP anchor (mm)	Length of CFRP anchor (mm)
	A	120	2×80	340
	B	80	2×80	260
SA1.0-CV	C	90	2×80	190
SA1.7-CVs	D	50	2×80	200
SA2.3-CCM	E	150	2×80	440
	F	60	2×80	220
	G	150	2×80	440

Figure 6 Test set-up and instrumentation.

cycle (cycle 6) were -44.4 kN and -0.06%, respectively. The first separation between the second storey panel and the first storey beam occurred at the 10th cycle. The pull load in this cycle was -81.0 kN (-0.19% drift), which was very close to the maximum pull load. The maximum loads for the forward and backward half cycles that the specimen could carry, were 83.7 kN (0.59% drift) and -86.2 kN (-0.38% drift), respectively. The base shear-roof drift diagram is shown in Figure 12.
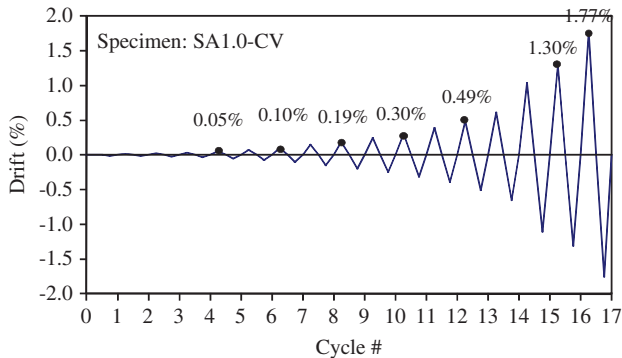
The failure is attributed to the formation of lap splice failure of column longitudinal bars, along with the axial tension failure of the vertical FRP strips, as shown in Figure 13. FRP

Figure 7 Displacement controlled loading regime for specimen SA1.0-CV.

flag configuration, at the corners of the masonry, impeded the crushing remarkably. On the other hand, the failure of the vertical strips led the specimen to a rocking and sliding type of movement, resulting in high distress on diagonal FRP strips. Sliding of the specimen at mid-height was observed after the failure of the vertical strips and before the failure of the diagonal ones. By contrast, sliding was not the predominant mode of failure. This sliding resulted in a so called pseudo-ductility on the pull part of the hysteretic curve.

4.3. Specimen SA2.3-CCM

The aspect ratio of this CFRP strengthened specimen was 2.3. The first visible hairline cracks were observed in the 8th cycle at the outer face of the left column, during the backward half cycle. The corresponding pull load and the drift were -52.0 kN and -0.020%, respectively. The first cracking on the infill was observed at the 9th cycle, at a pull load level of -55.3 kN (-0.023% drift). The first separation between the first storey panel and the beam took place at the 19th cycle, where the push load was 101.3 kN (0.15% drift). This load was approximately 71% of the specimen's lateral load capacity. In the subsequent cycles, following the infill cracking, stiffness degradation and roof displacements increased significantly, as shown in Figure 14.

Debonding of the cross diagonals was observed at the 22nd cycle, at an approximate drift level of 0.30%, and the
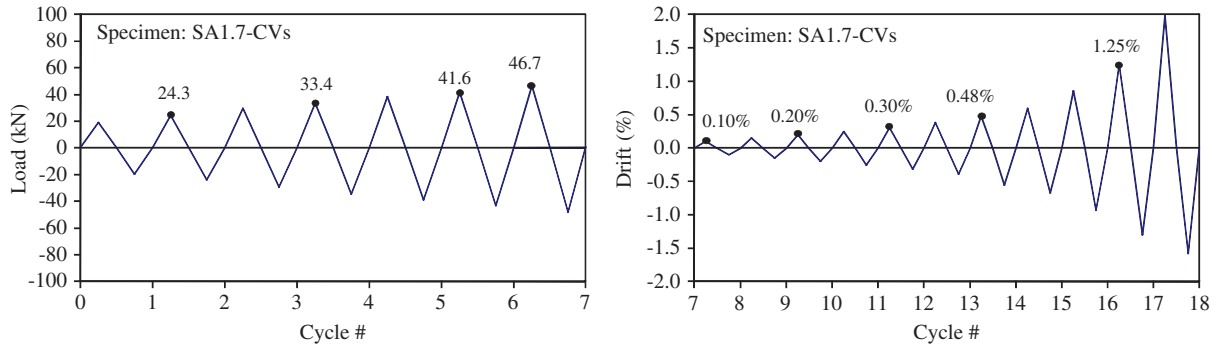
Figure 8 Loading regime for specimen SA1.7-CVs.

specimens carried extra load in the subsequent cycles, resulting from the stretching of the cross diagonals. The specimen's maximum load capacities for the forward and backward half cycles, were 142.3 kN (0.62% drift) and -143.2 kN (-0.77% drift), respectively. Rupturing of cross diagonals resulted in a significant load drop in the load carrying capacity, accelerated crushing, and deterioration. A sliding surface formed at the mid-height of the first storey panel, due to FRP orientation and reduction of the sliding surface at this specific height. Shear sliding type of failure at the mid-height of the first storey was followed by the gravity collapse of the columns under the combined action of shear, moment and axial forces as shown in Figure 15.

4.4. Modeling of infill

Based on the outcomes of the previous research [7–9, 11, 13] and the experimental results of the current study, a numerical model based on the equivalent diagonal strut concept, including the aspect ratio effect, was developed and proposed for the FRP strengthened infilled frames. The proposed uniaxial stress-strain relationship of the equivalent diagonal strut is illustrated in Figure 16. In this model, the FRP-strengthened infill wall is modeled as an equivalent diagonal compressive strut, with the same thickness of the infill panel. The effective width of the infill, w_{strut} is determined in accordance with Eq. (1) [18], where the variables γ and m are calculated in accordance with

Eqs. (2) and (3) [18]. It should be noted that these equations, later, were used by [19], with some editorial mistakes:

$$w_{strut} = \gamma \times \sqrt{L_{in}^2 + h_{in}^2} \times \sin 2\theta \tag{1}$$

$$\gamma = 0.32\sqrt{\sin 2\theta} \left[\frac{h^4 \times E_{in} \times t_{in}}{m \times E_c \times I_c \times h_{in}} \right]^{-0.1} \tag{2}$$

$$m = 6 \times \left[1 + \frac{6}{\pi} \arctan\left(\frac{E_b I_b h}{E_c I_c L_f} \right) \right] \tag{3}$$

although this effective width, w_{strut}, was developed for the initial stiffness of the infilled frames, the available literature shows that it was also used to find the ultimate capacity of the FRP-strengthened infill walls. The equivalent strut area, A_{strut}, can be calculated in accordance with Eq. (4).

$$A_{strut} = w_{strut} \times t_{strut} \tag{4}$$

Comparison of the test results of the study presented herein, and the previous work of Ozden et al. [13] (specimen U2 vs. SA1.7-CVs) and Atmaca [14] (SA1.0 vs. SA1.0-CV and SA2.3 vs. SA2.3-CCM), with the studies of Al-Chaar [7], revealed that the presence of FRP tended to increase the strength and the stiffness of the specimens. In order to
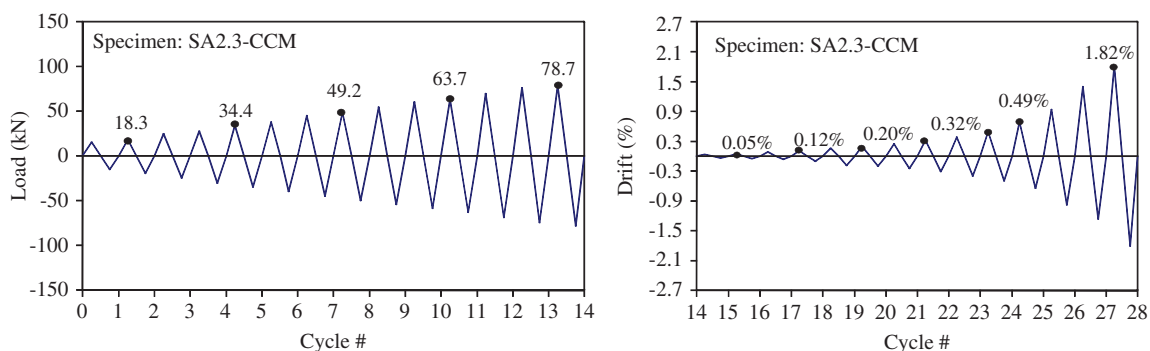

Figure 9 Loading regime for specimen SA2.3-CCM.

Figure 10 Damage state of specimen SA1.0-CV at 0.9% drift level.

$$k=\left[\frac{0.67}{(l/h)}\times\left(\frac{L_{flag}+L_{flag}+\sum W_{cross-diagonals}}{L_{diagonal}}\right)+1\right] \quad (5)$$
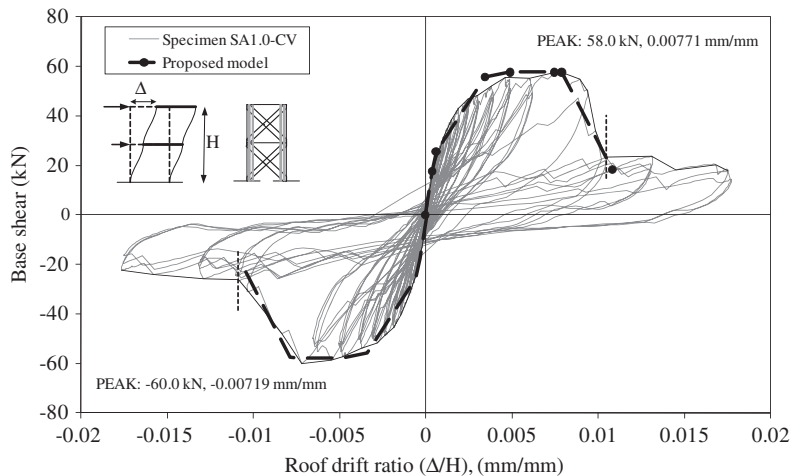
$$E_{bpmF}=k\times E_{bmp} \quad (6)$$

$$E_{bmp}=E_{bm}\times\frac{t_{bm}}{t_{bm}+2\times t_p}+E_p\times\frac{2\times t_p}{t_{bm}+2\times t_p} \quad (7)$$

where the modulus of elasticity of the brick infill, E_{bm} is calculated in accordance with UBC [20] as given in Eq. (8), in SI units. The modulus of elasticity for the plaster itself is calculated according to Eq. (9):
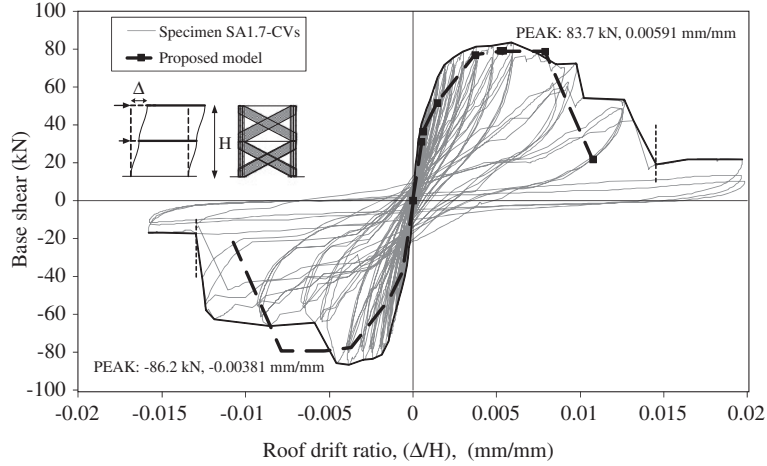
$$E_{bm}=750\times f_{bm}\leq20600 \quad (8)$$

$$E_p=5500\sqrt{f_p} \quad (9)$$

The f_{bm} and f_p are the compressive strength of brick infill wall calculated from the triplet tests, and compressive strength of plaster measured on 50 mm cubes, respectively. The capacity of the infill panels is calculated based on two possible failure modes, namely, corner crushing, and shear sliding. In literature, some other failure modes were also recorded, such as diagonal tensile cracking, out-of-plane failure or some FRP failure modes such as debonding, anchorage failure and rupturing [14, 21, 22]. However, diagonal tensile cracking is generally regarded as a serviceability limit state, since the system carries extra load beyond the level of diagonal cracking. In addition, out of plane failure is beyond the scope of this study. Thus, the failure modes were reduced to shear sliding and corner crushing of the infill panel for all specimens. The proposed diagonal compression strut approach inherently includes FRP failures, excluding the anchorage failure. In this study, three CFRP anchors were used on each end of

account for this effect in the numerical model, the modulus of elasticity of the strengthened infill is modified. The modification factor, k was a function of the frame's aspect ratio and calculated using Eq. (5). The modified modulus of elasticity was calculated in accordance with Eq. (6). The modulus of elasticity of the plastered infill wall (E_{bmp}) in Eq. (6) can be found in accordance with Eq. (7), which uses the rule of mixture:

Figure 11 Response of specimen SA1.0-CV.

Figure 12   Response of specimen SA1.7-CVs.

the diagonal FRPs, due to the larger width of the cross diagonals. A single CFRP anchor, on each end of the vertical strips, was used to fasten the vertical strips to the surrounding RC frame, due to the limited FRP width of 5 cm. It was assumed that approximately 40% of the CFRP material strength is utilized for the anchors of diagonal CFRP strips, hence, the total CFRP material used for the anchors was 2.4-fold of the CFRP width in the diagonal itself. The approximate effectiveness of the anchorage material for the vertical strips was assumed as 30%, resulting in a total CFRP cross-section of 3.2 times that of the vertical strip itself. The presence of wall anchorages decreased the un-bonded length, both for the vertical and diagonal strips in case of debonding, and this improved the performance of strengthened specimens.

Figure 13   Damage state of specimen SA1.7-CVs at 0.86% drift level.

The capacity of the proposed equivalent compression strut can be taken as the minimum of the shear sliding force in the strut direction, and the corner crushing load as given in Eq. (10):

$$R_{strut} = \min \left\{ \begin{array}{l} V_f / \cos\theta_{strut} \\ R_c \end{array} \right\} \qquad (10)$$

The maximum shear force, which is resisted by the panel itself, V_f, and the diagonal compression failure force, R_c, can be calculated as follows. The maximum shear force resisted by the panel (V_f) is calculated assuming that the vertical load on the infill panel is zero. The failure force of the FRP strips in all equations is calculated in accordance with Eq. (11). The average longitudinal strain in the FRP composite on the strengthened specimens (FRP impregnated with epoxy) is measured at an average value of $\varepsilon_{eff} = 0.0045$. Considering the approach defined in the FIB Bulletin 14 [23] and assuming a volume fraction of 35% fiber in the FRP composite and that the modulus of the fiber is 65-fold that of epoxy, the effective force developed by the FRP strip can be calculated through Eq. (11).

$$F_{strip} = t_{fiber} \times w_{strip} \times \sigma_{fiber} = t_{fiber} \times w_{strip} \times (0.0045 \times E_{fiber}) \qquad (11)$$

The following formulations are used to calculate V_f [Eq. (12)]. At first, all the shear is assumed to be taken by the infill; the lateral load capacity of the columns, either flexure or shear, is developed at further drift levels:

$$\begin{aligned} V_f = &\tau_{bm} \times l_{bmp} \times t_{bm} + \tau_p \times l_{bmp} \times 2 \times t_p + \mu \times R_s \times \sin\theta \\ &+ 2 \times \mu \times t_{frp\text{-}cross} \times b_{frp\text{-}cross} \times \sigma_{frp\text{-}cross} \times \sin\theta_{FRP} \\ &+ 4 \times \mu \times t_{frp\text{-}vertical} \times b_{frp\text{-}vertical} \times \sigma_{frp\text{-}vertical} \end{aligned} \qquad (12)$$

The diagonal compression strut force (R_s), as shown in Figure 17, is a function of the shear friction stresses, inclination of the strut (θ), and the aspect ratio of the frame. The summation of the horizontal component of R_s and the cross diagonal CFRP, can be assumed to be equal to the panel shear capacity as given in Eq. (13). It should be noted that Eq. (13) needs to be modified in the case of multiple strips:
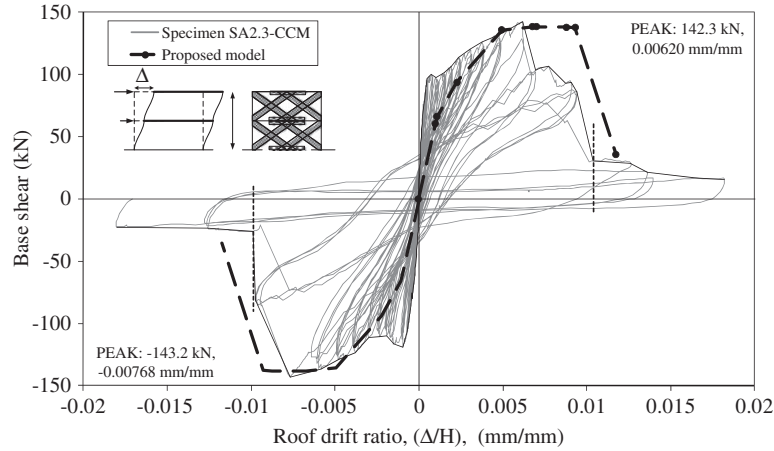
Figure 14   Response of specimen SA2.3-CCM.

$$V_f = R_s \times \cos\theta + 2 \times t_{frp\text{-}cross} \times b_{frp\text{-}cross} \times \sigma_{frp\text{-}cross} \times \cos\theta_{FRP} \qquad (13)$$

By equating the Eqs. (12) and (13), R_s can be written as given in Eq. (14):

$$R_s = \frac{1}{\cos\theta - \mu \times \sin\theta} \left\{ \begin{array}{l} \tau_{bm} \times l_{bmp} \times t_{bm} + \tau_p \times l_{bmp} \times 2 \times t_p \\ +2 \times \mu \times t_{frp\text{-}cross} \times b_{frp\text{-}cross} \times \sigma_{frp\text{-}cross} \times \sin\theta_{FRP} \\ +4 \times \mu \times t_{frp\text{-}vertical} \times b_{frp\text{-}vertical} \times \sigma_{frp\text{-}vertical} \\ -2 \times t_{frp\text{-}cross} \times b_{frp\text{-}cross} \times \sigma_{frp\text{-}cross} \times \cos\theta_{FRP} \end{array} \right\} \quad (14)$$

The diagonal compression strut force (R_s) for specimen SA2.3-CCM can be found using Eqs. (15), (16), and (17). These equations and free body diagrams of specimen SA2.3-CCM, as indicated in Figure 18, are submitted for clarification:

$$V_f = \tau_{bm} \times l_{bmp} \times t_{bm} + \tau_p \times l_{bmp} \times 2 \times t_p + \mu \times R_s \times \sin\theta \\ + \sum_{i=1}^{2} 2 \times \mu \times t_{frp\text{-}i} \times b_{frp\text{-}cross\text{-}i} \times \sigma_{frp\text{-}cross\text{-}i} \times \sin\theta_{FRP\text{-}i} \qquad (15)$$

$$V_f = R_s \times \cos\theta + \sum_{i=1}^{2} 2 \times t_{frp\text{-}i} \times b_{frp\text{-}cross\text{-}i} \times \sigma_{frp\text{-}cross\text{-}i} \times \cos\theta_{FRP\text{-}i} \qquad (16)$$

$$R_s = \frac{1}{\cos\theta - \mu \times \sin\theta} \left\{ \begin{array}{l} \tau_{bm} \times l_{bmp} \times t_{bm} + \tau_p \times l_{bmp} \times 2 \times t_p \\ + \sum_{i=1}^{2} 2 \times \mu \times t_{frp\text{-}i} \times b_{frp\text{-}cross\text{-}i} \times \sigma_{frp\text{-}cross\text{-}i} \times \sin\theta_{FRP\text{-}i} \\ - \sum_{i=1}^{2} 2 \times t_{frp\text{-}i} \times b_{frp\text{-}cross\text{-}i} \times \sigma_{frp\text{-}cross\text{-}i} \times \cos\theta_{FRP\text{-}i} \end{array} \right\} \\ \qquad (17)$$

Diagonal compression failure force, R_c (Eq. 20), on the other hand, is directly proportional to the compressive strength of the strengthened masonry (f_{bmpF}) and the contact length (z_{clm}) between panel and the column as given in Eqs. (18)–(20). The factor "k" is the modification factor for the strength and stiffness enhancements, and is calculated according to Eq. (5):

$$z_{clm} = \frac{\pi}{2} \left(\frac{4 \times E_c \times I_c \times h_{bmp}}{E_{bmp} \times t_{bmp} \times \sin 2\theta} \right)^{\frac{1}{4}} \qquad (18)$$

Figure 15   Damage state of specimen SA2.3-CCM at the end of loading scheme.
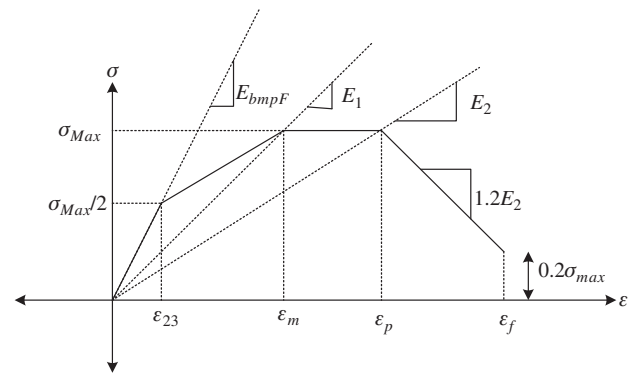

Figure 16   Axial stress-axial strain relationship of the equivalent compression strut.

$$f_{bmpF} = \left[f_{bm} \times \frac{t_{bm}}{t_{bm}+2 \times t_p} + f_p \times \frac{2 \times t_p}{t_{bm}+2 \times t_p} \right] \times k \qquad (19)$$

$$R_c = \frac{2}{3} \times z_{clm} \times t_{bmp} \times f_{bmpF} \times \sec \theta \qquad (20)$$

Ultimate stress (σ_{max}) resisted by the equivalent compression strut, as shown in Figure 16, can be found by dividing the strut capacity, R_{strut} [Eq. (10)] by the cross-sectional area of the compression strut, A_{strut} [(Eq. (4)] as given in Eq. (21). The modification implemented for the ultimate stress, includes the aspect ratio effect, AR. The test results yielded that the strain attained at maximum stress level is influenced by both the existence of FRP and the aspect ratio of the frame. Therefore, the strain at maximum stress, ε_m, was calibrated by test results and given in Eq. (22). The first crushing strain for non-strengthened infill walls, ε_0, is given in Eq. (23):

$$\sigma_{max} = (0.7 + 0.3AR) \times R_{strut}/A_{strut} \qquad (21)$$

$$\varepsilon_m = \frac{k\varepsilon_0}{AR} \qquad (22)$$

$$\varepsilon_0 = 0.0024 \times \ln(AR) + 0.0011 \qquad (23)$$

The capacity of the diagonal compression strut is assumed constant, between ε_m and the post peak strain, ε_p (Figure 16). It should be noted that the ε_p strain level is closely related to the frame aspect ratio, AR [Eq. (24)] and inherently related to the effectiveness of the FRP, which in the text is referred to as the modification factor, k.

Figure 17 Forces acting on the specimens SA1.0-CV and SA1.7-CVs.

$$\varepsilon_p = 4\varepsilon_m \frac{AR}{(1.4AR-0.4)} \qquad (24)$$

If there is no strengthening, the post peak strain, ε_p, and the maximum strain, ε_m, would be equal to each other (Figure 16). The negative slope of the proposed curve is suggested as $1.2*E_2$ (Figure 16). Although this negative slope was recommended as a function of the initial slope in the literature [8], test data of the current study yields a better correlation with the secant modulus of elasticity, at post peak strain. It is assumed that the failure strain of the compression strut is reached when the stress decreases to 20% of the maximum, σ_{max}. Once the stress-strain relation is established, the axial load-axial deformation relation can easily be derived by multiplying strains and stresses with the initial length of the strut and initial area of the strut, respectively.

The macro model, incorporating the proposed infill model, is shown in Figure 19. Plastic hinges were defined, where nonlinearities are expected; such as at the ends of frame members and at the mid-length of the equivalent compression strut. The plastic hinges on the columns and beams included moment, axial and shear effects independently. The infill model included a plastic hinge at the middle part, as shown in Figure 19. Moment-curvature (M3 hinge), axial stress-axial strain (P hinge) and shear stress-shear strain (V2 hinge) relations were defined to model the plastic hinges. Frame members were modeled as elastic members with cracked flexural rigidity, which was the initial slope of the bilinear moment-curvature diagrams. Rigid end zones, to account for joint rigidities, were defined at the ends of the frame members. Plastic hinge lengths for the flexural hinges, were 50 mm for columns and 75 mm for beams; half of the section height. Plastic hinge lengths accounting for nonlinearities due to shear and axial stresses were equal to the clear length of the members considered (column, beam and strut). Based on the above explanations, a nonlinear static analysis (pushover analysis) was carried out and compared with the test results. The negative effect of lap splices in columns is addressed by reducing the moment capacity by a factor of lap splice deficiency over the code specified value. Similarly, the curvature ductility was also reduced accordingly.

4.5. Comparison of experimental and theoretical results

The infill model described above was used to generate the load displacement graphs of the tested specimens. The base shear-roof drift ratio diagrams of the specimens SA1.0-CV, SA1.7-CVs and SA 2.3-CCM, are given in Figures 11, 12 and 14, respectively.

Tensile failure of the columns, and rupturing of vertical FRPs, resulted in the failure of specimen SA1.0-CV, and severe post-peak strength degradation observed, as shown in Figure 11. The proposed model could satisfactorily predict the pre-peak and post-peak behavior. It is believed that the good correlation between the envelope of the experimental curve and the nonlinear model of the equivalent strut was due to the fact that strengthened infill properties governed the failure
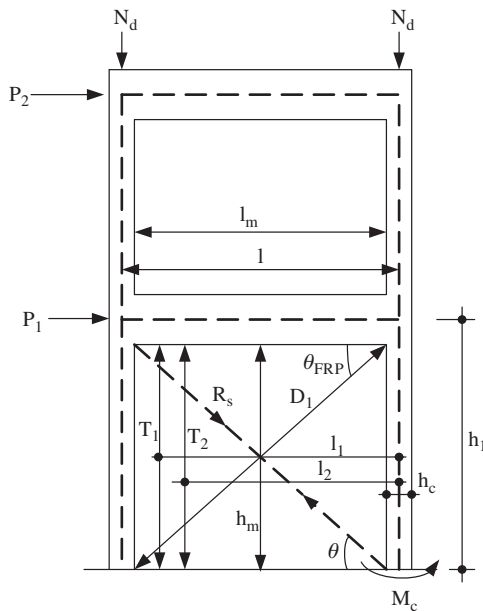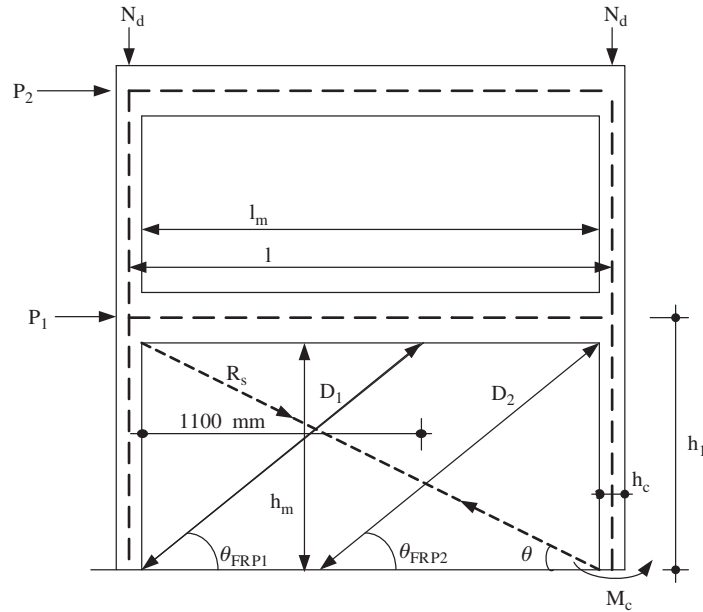
Figure 18 Forces acting on the specimen SA2.3-CCM.

mode. The first cracking loads, experimental and analytical, were quite close to each other. The first stiffness change in the analytical curve was at a load level of 17.7 kN, showing the initial cracking, while the experimentally observed first cracking load was 21.2 kN. Peak loads were almost the same, as shown in Figure 11. Initial stiffness and secant stiffness at the peak load of the analytically obtained envelope curve, were 28.7 kN/mm and 4.6 kN/mm, respectively. The experimentally obtained values were 31.64 kN/mm and 4.64 kN/mm in turn. The areas under the experimentally and analytically obtained envelope curves, a good indicator for the dissipated energy, were 0.996 kNmm/mm and 0.980 kNmm/mm. It should be noted, that these numbers were obtained from base shear-roof drift ratio graphs. Thus, they did not represent the real dissipated energy. The results of specimen SA1.0-CV showed that the pushover analysis, and the proposed model, can satisfactorily predict the behavior including post peak strength degradation.

The failure of specimen SA1.7-CVs was due to the combined action of rocking and sliding at the first storey mid-height, and also shear and tensile failure of the columns, resulting in a rather mixed failure. In the model, failure of the equivalent compression strut and flexural hinging of column bases were obtained. The comparison of the model and experimental envelope curves are shown in Figure 12. The vertical thin dashed lines in Figures 11, 12 and 14, represent the last points on the experimental envelope curves up to which the dissipated energy was calculated. Experimental and analytical peak loads were 83.7 kN and 79.3 kN, respectively. Initial stiffness and secant stiffness at the peak load of the model were 36.3 kN/mm and 8.6 kN/mm, respectively, whereas the corresponding experimental values were 64.79 kN/mm and 7.33 kN/mm. The areas under the model and experimental backbone curves were 1.34 kNmm/mm and 1.80 kNmm/mm,

respectively. The ratio is about 0.75. The first cracking loads of the model and the test were 31.6 kN and 36 kN, respectively. The stepwise stiffness change along the analytical curve, is closely affected by the sequence of member hinging. The initial stiffness observed in Figure 12 slightly changes with the hinging of column bases. By contrast, the hinging of diagonal compression strut resulted in severe stiffness changes.

In specimen SA2.3-CCM, a shear sliding type of failure was observed in the test. The model captured this failure mode, as well as the failure load, satisfactorily. Base shear versus roof drift diagram of specimen SA2.3-CCM is shown in Figure 14. The initial stiffness and secant stiffness at the peak load for the model were 36.0 kN/mm and 11.5 kN/mm, respectively, whereas the initial stiffness and stiffness at the peak load of the experimentally obtained envelop curve, were calculated as 204 kN/mm and 13.4 kN/mm, respectively. The model was unable to predict the initial stiffness satisfactorily. Stiffness at the peak load of the model was close to that of the test. The areas under envelope curves for the model and the test were 2.50 kNmm/mm and 2.27 kNmm/mm, respectively. First cracking loads of the model and test were 60.8 kN and 49.7 kN, respectively. The model for this specimen was satisfactory for the quick evaluation process, considering the capacity and post peak degradation.

5. Conclusions

This paper presents the experimental results for the aspect ratio effect on the strengthened infilled frames. In addition, an equivalent compression strut model, including the effect of the aspect ratio, was proposed and tested against the experimental results in terms of strength, stiffness and post peak behavior. The model did not include the changes in the effective widths. The initial stiffness calculations were based on
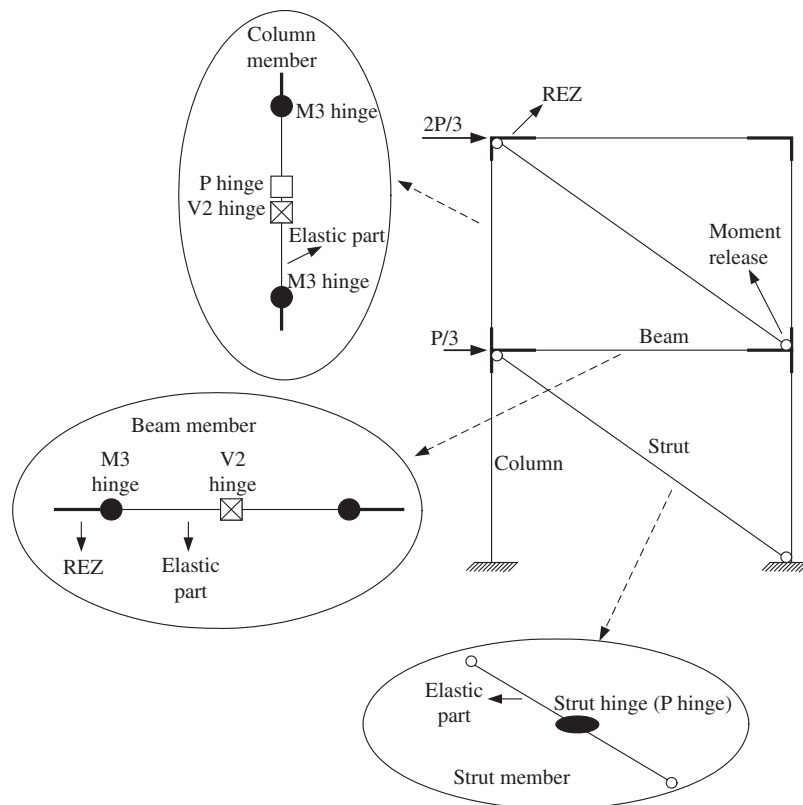
Figure 19   Mathematical model of the specimens.

the equivalent strut concept. Based on this study, the following conclusions are drawn.

Building strengthening with CFRP overlays, can be considered to be rapid and effective, however, the efficiency and failure modes are strongly influenced by the aspect ratio of the strengthened frames. Besides, the preparation of CFRP anchors and anchor holes has prime importance in achieving the optimum efficiency of this strengthening technique, as verified by the test results.

The aspect ratio of the specimens influences the failure modes significantly. Mid-height rocking action was dominant in the behavior of SA1.0-CV (aspect ratio=1) whereas the shear sliding type of behavior was predominant in the behavior of specimen SA2.3-CCM (aspect ratio=2.3). The test results proved that the vertical strips on the infill wall are much more effective for small aspect ratios. However, the vertical strip ratio was not enough to eliminate thoroughly the lap splice deficiency of the columns of SA1.0-CV.

The load carrying mechanism for the FRP-strengthened infilled frames was mainly the combined action of the frame response, the shear and diagonal compression response of the infill panel, and the diagonal tension produced by the FRP strips on the masonry wall. The rupturing of FRP strips transferred this mechanism into a frame only system, where the surrounding frame was not designed for such high loads. A change in the response results in a significant drop in the lateral load capacity.

The proposed model, which replaced the FRP-strengthened infill wall with a pin connected equivalent diagonal compression strut, includes the aspect ratio effect. The model uses a single equivalent diagonal compressive strut, different from other strut and tie models. The capacity and behavior of the specimens with similar strengthening schemes were predicted satisfactorily. The ratios between analytically and experimentally obtained capacities of the specimens SA1.0-CV, SA1.7-CVs and SA2.3-CCM were 0.99, 0.95, and 0.97, respectively.

Acknowledgements

Notation

AR	Frame aspect ratio
A_{strut}	Cross-sectional area of compressive strut
$b_{frp\text{-}cross}$	Width of the cross diagonal CFRP overlay
$b_{frp\text{-}vertical}$	Width of the vertical CFRP overlay

E_{fiber}	Producer specified modulus of elasticity of CFRP (MPa)	$\sigma_{frp\text{-}vertical}$	Tensile stress on vertical CFRP strip developed at a strain level of 0.0045
E_{bm}	Modulus of elasticity of brick infill excluding plaster	σ_{max}	Maximum compressive stress carried by the infill compressive strut
E_{bmp}, E_{in}	Modulus of elasticity of brick infill including plaster	θ	The angle between diagonal of the panel and horizontal axis
$E_b I_b$	Flexural stiffness of the beam	θ_{FRP}	Inclination of the cross FRP diagonals with respect to horizontal axis
$E_c I_c$	Flexural stiffness of the column	τ_{bm}	Shear strength of brick infill wall excluding plaster [$=(0.0133{\times}f_p+1.3783){\times}0.30$]
E_p	Modulus of elasticity of plaster		
E_s	Modulus of elasticity of steel	τ_p	Shear strength of plaster [$=(0.15{\times}f_p){\times}0.30$]
f_{bm}	Compressive strength of brick wall, measured from triplet tests (MPa)		

All units are MPa and mm unless otherwise specified.

f_{bmpF}	Compressive strength of the CFRP strengthened masonry
f'_c	Concrete compressive strength (on 150×300 cylinder specimen)
f_p	Compressive strength of plaster, measured on 5×5×5 cm cubes
f_{ult}	Ultimate tensile strength of overlaying fiber
f_{yk}	Yield strength of steel
f_{ywk}	Yield strength of transverse steel
h, h_1	Storey height
h_{in}, L_{in}, t_{in}	Height, length and thickness of the masonry infill panel
h_m, h_{bmp}	Height of the infill panel
k	Modification factor
l, L_f	Frame span length, column center to center
l_{bmp}, l_m	The clear bay length of the wall
$L_{diagonal}$	Diagonal length of the infill panel
L_{flag}	Length of the infill diagonal covered by the CFRP corner flags
R_c	Compression failure load of the diagonal strut (kN)
R_{strut}	Strut capacity (minimum of shear sliding or corner crushing)
t_{bm}	Thickness of brick wall excluding plaster
t_{fiber}, $t_{frp\text{-}cross}$	Thickness of the CFRP overlay aligned on the infill diagonal
t_{fiber}, $t_{frp\text{-}vertical}$	Thickness of the vertical CFRP overlay
t_p	Thickness of plaster (on one side only)
t_{strut}, t_{in}, t_{bmp}	Thickness of the strut including plaster ($t_{strut}=t_{bm}+2{*}t_p$)
V_f	Maximum shear force resisted by the infill panel (kN)
$W_{cross\text{-}diagonal}$	Length of the infill diagonal covered by the transverse X CFRP diagonal
w_{strut}	Effective equivalent strut width
z_{clm}	Contact length between panel and the column
ε_m	Maximum strain on the compressive strut attained when σ_{max} is reached
ε_o	First crushing strain of the compressive strut
ε_p	Post peak strain of the compressive strut
ε_{ult}	Failure tensile strain for the overlaying fiber
ε_{23}	Strain on the compression strut when $\sigma_{max}/2$ is reached (use E_{bmpF})
μ	Coefficient of friction (taken as 0.3)
$\sigma_{frp\text{-}cross}$	Tensile stress on cross diagonal developed at a strain level of 0.0045

References

[1] Ehsani MR, Saadatmanesh H, Al-Saidy A. *ASCE J. Compos. Constr.* 1997, 1, 17–25.

[2] Triantafillou TC. *ASCE J. Compos. Constr.* 1998, 2, 96–104.

[3] Velazquez-Dimas JI, Ehsani MR, Saadatmanesh H. *ACI Struct. J.* 2000, 97, 377–387.

[4] Valluzzi MR, Tinazzi D, Modena C. *Constr. Build. Mater.* 2002, 16, 409–416.

[5] Marshall OS, Sweeney SC, Trovillion JC. *Performance Testing of Fiber-Reinforced Polymer Composite Overlays for Seismic Rehabilitation of Unreinforced Masonry Walls.* Technical Report, US Army Corps of Engineers, ERDC/CERL TR-00-18, 2000.

[6] ElGawady MA, Lestuzzi P, Badoux M. *ASCE J. Compos. Constr.* 2007, 11, 50–61.

[7] Al-Chaar GK, Lamb GE. *Design of Fiber Reinforced Polymer Materials for Seismic Rehabilitation of Infilled Concrete Structures.* Technical Report, US Army Corps of Engineers, Technical Report, ERDC/CERL TR-02-33, 2002.

[8] El-Dakhakhni WW. *Experimental and Analytical Seismic Evaluation of Concrete Masonry-Infilled Steel Frames Retrofitted Using GFRP Laminates.* PhD Dissertation, Drexel University, 2002.

[9] Hakam ZH-R. *Retrofit of Hollow Concrete Masonry Infilled Steel Frames Using Glass Fiber Reinforced Plastic Laminates.* PhD Dissertation, Drexel University, 2000.

[10] Erdem I, Akyuz U, Ersoy U, Ozcebe G. *Eng. Struct.* 2006, 28, 1843–1851.

[11] Hanoglu KB. *Fiber Reinforced Plastic Overlay Retrofit of Hollow Clay Tile Masonry Infilled Reinforced Concrete Frames.* PhD Dissertation, Department of Civil Engineering, Bogazici University, 2002.

[12] Yuksel E, Ilki A, Erol G, Demir C, Karadogan HF. In *Advances in Earthquake Engineering for Urban Risk Reduction*, Wasti, ST, Ozcebe, G, Eds., Springer: Amsterdam, The Netherlands, 2006, pp. 285–300.

[13] Ozden S, Akguzel U, Ozturan T. *ACI Struct. J.* 2011, 108, 414–422.

[14] Atmaca S. *Strengthening of Brick Infilled RC Frames with Different Aspect Ratios by Means of CFRP Overlays.* PhD Dissertation, Department of Civil Engineering, Bogazici University, 2008.

[15] American Society for Testing and Materials, ASTM C39-96. *Standard Test Method for Compressive Strength of Cylindrical Concrete Specimens.* Annual Book of ASTM Standards, Vol. 04.02, West Conshohocken, PA, 1997.

[16] American Society for Testing and Materials, ASTM E447-97. *Standard Test Method for Compressive Strength of Laboratory*

Constructed Masonry Prisms. Annual Book of ASTM Standards, Vol. 04.05, West Conshohocken, PA, 1997.

[17] ACI T1.1-01 *Acceptance Criteria for Moment Frames Based on Structural Testing*. American Concrete Institute, Farmington Hills, MI, 2001.

[18] Durrani AJ, Lou YH. *Seismic Retrofit of Flat-Slab Buildings with Masonry Infills*. NCEER Workshop on Seismic Response of Masonry Walls, Technical Report, NCEER-94-0004, San Francisco, CA, 1994.

[19] Perera R. *Eng. Struct*. 2005, 27, 1278–1288.

[20] UBC. "*Uniform Building Code: Vol. 2, Structural Engineering Design Provisions*". International Conferences of Building Officials, Whittier, CA, 1997.

[21] FEMA 306. *Evaluation of Earthquake Damaged Concrete and Masonry Wall Buildings.* Applied Technology Council, Redwood City, CA, 1998.

[22] El-Dakhakhni WW, Elgaaly M, Hamid AA. *ASCE J. Struct. Eng*. 2003, 129, 177–185.

[23] FIB. *Externally Bonded FRP Reinforcement for RC Structures.* Lausanne, Technical Report, Bulletin 14, 2001.